



Contents lists available at ScienceDirect

International Journal of Solids and Structures

journal homepage: www.elsevier.com/locate/ijsolstr

3D mechanics of scaled membranes

Ali Shafiei^a, Francois Barthelat^{a,b,*}^a Department of Mechanical Engineering, McGill University, 817 Sherbrooke Street West, Montreal, QC H3A 2K6, Canada^b Department of Mechanical Engineering, University of Colorado, 427 UCB, 1111 Engineering Dr, Boulder, CO 80309, United States

ARTICLE INFO

Keywords:

Bioinspiration
3D discrete element method
Segmented hard material
Puncture resistance
Flexural compliance

ABSTRACT

Scale-covered skins are excellent examples of natural flexible protective systems. With segmented hard scales bonded or embedded onto a deformable skin, these natural structures provide useful combinations of puncture resistance and flexural compliance. The interaction of the scales with the substrate and the scales themselves is the key to such high-performance systems. In this work we investigate the 3D mechanics of puncture and flexion for a range of designs for scale-covered systems, using validated discrete element models (DEM) of the scales. The scales are orders of magnitude harder and stiffer than the substrate, so that they can be considered rigid for the purpose of mechanical modeling. Our main findings are that scales with no slant angles positioned in arrays increase puncture resistance compared to isolated scales, but only by way of interactions through the substrate and with much less extent by direct contact between scale. Direct scale-scale interaction can however be much improved by slanting the scales which we also examined in this work. We also examined the in-plane kinematics of scales, and identified interlocking mechanisms between rows of scales that further increase toughness. Dart- and hexagon-shape scales combined all these mechanisms in the most effective way among the designs we explored here. This study provides new insights into the effect of the base shape and the slant angle of the scales on the mechanical behavior of scale-covered systems, which in turn can help in the design and optimization of improved protective systems.

1. Introduction

Natural materials often combine very hard and very soft components, in specific architectures that generate outstanding mechanical performance (Wegst, 2014; Chen et al., 2012; Rajabi et al., 2016; Chen et al., 2011; Barthelat, 2015). For example the skin of fish, armadillos or crocodiles consist of discrete hard scales which are orders of magnitude stiffer than the surrounding tissues and bare skin (Chen et al., 2011; Chintapalli et al., 2014; Zhu et al., 2012). This specific construction enables high surface hardness and protection, while minimizing hindrance and enabling agile locomotion (Chen et al., 2011; Yang et al., 2013; Vernerey and Barthelat, 2014; Rudykh and Boyce, 2014). Individual scales can also interact with each other by direct contact, which increases puncture resistance (Yang et al., 2013; Szewciw and Barthelat, 2017; Vernerey et al., 2014). In fish skin, the scales are slanted and have overlaps which promote scale-scale interactions (Vernerey and Barthelat, 2010; Ghosh et al., 2014; Ghosh et al., 2016). These contacts promote the distribution of highly localized puncture forces over wider areas, which can prevent blunt trauma to underlying tissue (Martini and

Barthelat, 2016; Zhu et al., 2013; Browning et al., 2013; Tatari et al., 2020). The construction and mechanics of fish scales and other dermal armors have been the focus of numerous studies on the effect of the geometry and arrangement of the scales on the mechanical performance, with a strong focus on puncture resistance and on flexural compliance, two mechanical properties which have been shown to be mutually exclusive (Chintapalli et al., 2014; Vernerey and Barthelat, 2014; Rudykh and Boyce, 2014; Vernerey et al., 2014; Martini and Barthelat, 2016; Browning et al., 2013; Funk et al., 2015; Martini et al., 2017; Rudykh et al., 2015; Shafiei et al., 2021). Failure of a scaled skin may occur in one of two ways: by fracturing or puncturing individual scales, or by unstable tilting of the scales (Yang et al., 2013; Martini and Barthelat, 2016; Martini and Barthelat, 2016; Connors et al., 2019). Fracturing individual scales is delayed by the strength and toughness of individual scales (Ghods et al., ; Murcia et al., 2015; Ghods et al., 2019), while unstable tilting can be delayed by direct contact between the scales (Browning et al., 2013; Martini et al., 2017; Shafiei et al., 2021) (in particular for configurations where scales overlap (Yang et al., 2013; Martini and Barthelat, 2016; Shafiei et al., 2021). To this effect,

* Corresponding author at: Department of Mechanical Engineering, McGill University, 817 Sherbrooke Street West, Montreal, QC H3A 2K6, Canada.

E-mail address: francois.barthelat@colorado.edu (F. Barthelat).

<https://doi.org/10.1016/j.ijsolstr.2022.111498>

Received 19 April 2021; Received in revised form 11 January 2022; Accepted 7 February 2022

Available online 9 February 2022

0020-7683/© 2022 Published by Elsevier Ltd.

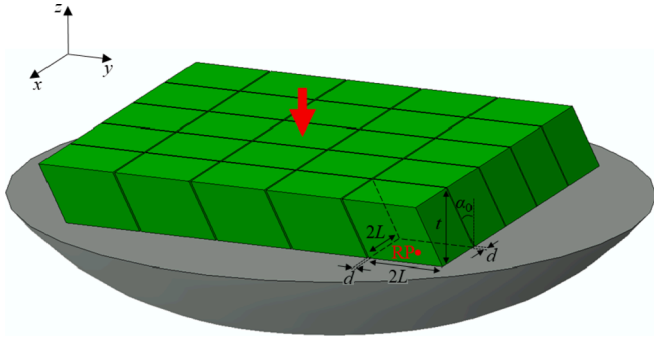


Fig. 1. Typical system considered in this study: 5×5 Array of hard scales bonded to a soft substrate and subjected to puncture. Key dimensions for individual scales are shown.

experiments suggested that the shape and the arrangement of the scales had a significant effect on the puncture resistance and flexural compliance of the system (Yang et al., 2013; Martini et al., 2017; Rudykh et al., 2015; Connors et al., 2019). Experimental studies on 3D designs are however limited in terms of the geometries explored, so that the effect of the shapes and the arrangement of the scales on the mechanical behaviour of the system is not fully understood yet. The interaction of the scales in 3D may also be captured with numerical models, but typical method such as finite elements require a large number of contact elements and a multitude of contact pairs which are computationally expensive and which can even prevent numerical convergence (Shafiei et al., 2021; Dugué et al., 2013; Ghosh et al., 2017). In our recent work (Shafiei et al., 2021), we developed a 2D DEM model to investigate the mechanical performance of scale-covered-structures. While these models could capture some basic mechanisms of scale-scale interaction and scale-substrate interaction, they could not capture the effect of the 3D shapes of the scales, the 3D arrangement and the slant angle of the scales and the interlocking mechanism between the neighboring scales on surface of the skin. Here we developed and explored 3D models of the scale to capture these effects and mechanisms. We used a three-dimensional formulation of the discrete element method (DEM) where individual scales are assumed to be rigid, with linear springs used to model the interactions of the scales with the substrate (Shafiei et al., 2021; Abid et al., 2018; Abid et al., 2019; Pro and Barthelat, 2020; Bolander and Saito, 1998). After validating with experiments, we investigated the mechanical behaviour of scale-covered system with a variety of scale shapes and arrangements.

2. Modeling and validation

For this study, we investigated the puncture resistance of a 3D model of identical hard scales fully bonded onto a soft substrate which was modeled as a linear elastic half-space (Young's modulus E_s , Poisson's ratio ν_s). We first modeled some of the configurations examined experimentally in our previous study (Martini et al., 2017): Slanted square scales arranged in a square array and with overlap generated by the slanted sides of the scales (Fig. 1). Each scale was constructed from a square base with the size $2L \times 2L$, extruded in the out-of-plane direction by a thickness t and following a slant angle α_0 towards the x -direction. This approach to creating the scales was in line with our previous experiments (Martini et al., 2017) where different scale geometries were generated based on simple variations a simple cubic scale. The advantage of this approach is that the geometry of the scales can be easily by characterized by the geometry of the base surface, slant angle and thickness. The scales were arranged in a square array with a uniform gap distance d (Fig. 1). To fully cover the substrate with the scales we assumed the gap distance to be very small compared to the sizes of the scales ($d/L = 0.005$, to avoid convergence issues one must have $d > 0$). The objective was to model stiff scales, which are several orders of

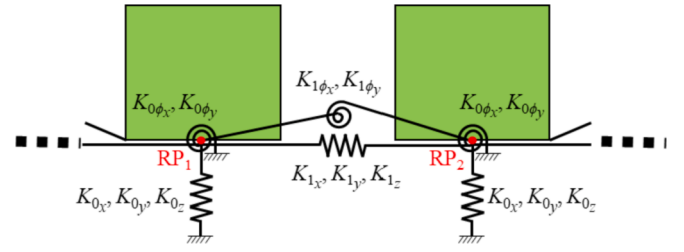


Fig. 2. Setup of linear springs captures the interactions of individual scales with the substrate, and also the interactions between neighboring scales through the substrate.

magnitude stiffer than the substrate, and therefore the scales were modeled as rigid blocks (Zhu et al., 2012; Shafiei et al., 2021). The sharp puncture experiment on the scaled system was duplicated in the model by applying a vertical displacement into the center of central scale in the model (red arrow in Fig. 1).

We used the 3D discrete element modeling capability of ABAQUS/CAE to capture the puncture mechanics of this system. Individual scales consisted of six faces where each face was made of a 4-node discrete rigid element R3D4. The displacement and rotations of the six face elements were defined in relation to a reference framework centered on a reference point associated with each scale which we placed at the centroid of the basal face of the scale (point RP on Fig. 1). The reference points were given five degrees of freedom: translation in x -, y -, z -directions, and rotation about the x - and y -axes. Since experiments mainly showed scale rotations about the x - and y -axes and negligible rotation about the z -axis (out of plane axis), that rotation was maintained to zero during the simulations to facilitate numerical convergence. To apply puncture forces to individual scales, a node was created on the top surface of the punctured scale as the loading point. A rigid connector then was defined between the loading point and the reference point of the scale, and a controlled vertical displacement was applied to the loading point (red arrow in Fig. 1). Through the rigid connector, the applied displacement and the resulting force were transferred to the reference point of the punctured scale. The model captured the interaction of individual scales with the substrate with a system of linear springs (Fig. 2). Some of the springs captured the elastic interaction of individual scales with the substrate, and other captured the elastic interactions of each scale with its neighbors through the substrates. The scales can indeed interact through the substrate. For example displacing an individual scale deforms the substrate, which can in turn displace other neighboring scales. This interaction between neighboring scales (which may not necessary enter contact) depend on the distance between the scale and on the elasticity of the substrate. The system of springs was set as follows: The reference point of each scale was connected to the ground (a reference plane "far below" the surface of the substrate) by two-node connector element CONN3D2 with extensional and rotational stiffness coefficients K_{0x} , K_{0y} , K_{0z} , $K_{0\phi_x}$ and $K_{0\phi_y}$. Neighbouring scales were connected by their reference points by a two-node connector element CONN3D2 with "interaction" stiffness coefficients K_{1x} , K_{1y} , K_{1z} , $K_{1\phi_x}$ and $K_{1\phi_y}$. We then calibrate the stiffness coefficients using Boussinesq's and Cerruti's closed-form solutions for point forces on an elastic half-space (Shafiei et al., 2021; Barber, 2002; Okumura, 1995). For example, to obtain the coefficients K_{1x} and K_{0x} , we applied a tangential displacement u_x to the central scale while keeping all other scales immobile. The distributed shear load $q_x(x,y)$ on the surface of the substrate underneath the scales in x -direction was computed using (Shafiei et al., 2021):

$$u_x = \frac{1+\nu_s}{\pi E_s} \iint q_x(\zeta, \gamma) \left[\frac{1-\nu_s}{\sqrt{(x-\zeta)^2 + (y-\gamma)^2}} + \frac{\nu_s(x-\zeta)^2}{\sqrt{((x-\zeta)^2 + (y-\gamma)^2)^3}} \right] d\zeta d\gamma \quad (1)$$

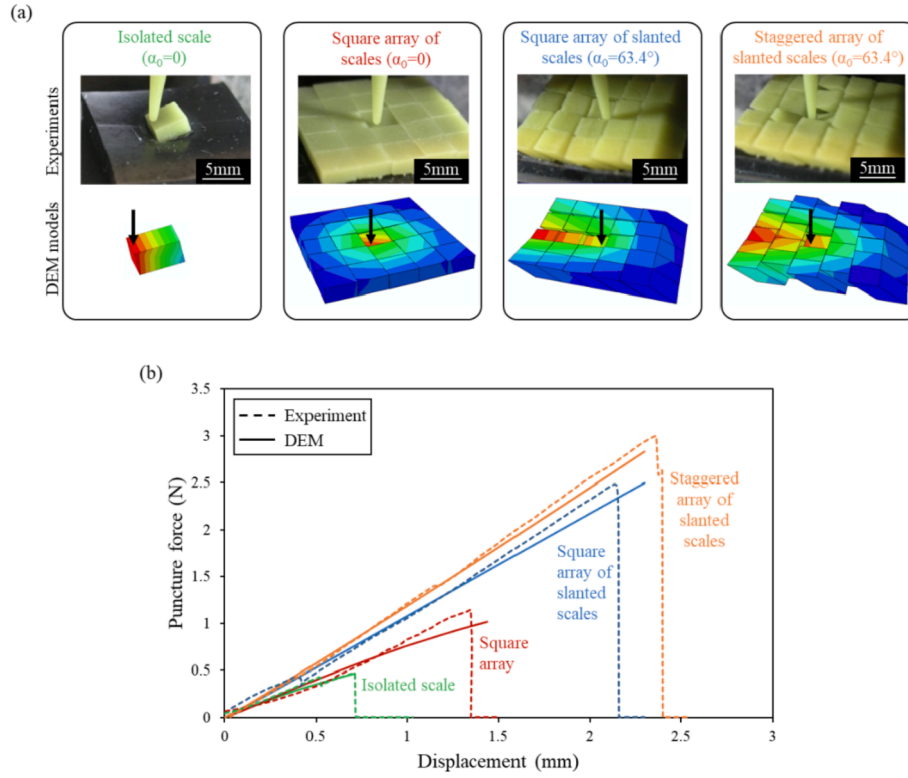


Fig. 3. (a) Snapshots of experiments and models for a puncture test on four different designs; (b) Corresponding puncture force–displacement curves showing a good agreement between models and experiments.

where ζ and γ are the integral variables in x - and y -directions, respectively. We then integrated the shear load $q_x(x,y)$ over the area of the scales to get the shear force on each scale including the middle and the neighboring scales (the integration is calculated over the areas of the substrate underneath the scales on the intervals of $[0, 2L]$, $[2L + d, 4L + d]$ and $[4L + 2d, 6L + 2d]$ in both x - and y -directions), which divided by the applied displacement of u_x produced the stiffness coefficients K_{0x} and K_{1x} . The same approach was used to calibrate K_{0y} and K_{1y} , except we applied a displacement u_y to the central scale to compute the shear load $q_y(x,y)$ in the y -direction. To obtain K_{0z} and K_{1z} , we imposed a normal displacement u_z to the central scale and computed the normal distributed load $p(\zeta,\gamma)$ on the surface of the substrate underneath the scales using (Shafiei et al., 2021):

$$u_z = \frac{1 - \nu_s^2}{\pi E_s} \iint p(\zeta,\gamma) \frac{1}{\sqrt{(x-\zeta)^2 + (y-\gamma)^2}} d\zeta d\gamma \quad (2)$$

We applied a rotation ϕ_x about the x -axis to the central scale, used equations (1) and (2) to obtain the distributed shear and normal loads ($q_y(x,y)$ and $p(x,y)$), and calculated the resultant moment for each scale (Shafiei et al., 2021). We divided the moment on the central scale and on the neighbouring scales by the imposed rotations about either x -axis or y -axis to obtain the stiffness coefficients $K_{0\phi_x}$; $K_{1\phi_x}$, $K_{0\phi_y}$ and $K_{1\phi_y}$ respectively. Fig. 1

In addition to interacting through the substrate, scales can also interact by direct contact with their neighbors. For our model we defined a frictionless contact with a linear penalty method where the contact force is proportional to the interpenetration distance between the scales. Once the model was in place and all parameters calibrated, we compared its predictions with our previous experiments (Martini et al., 2017) which consisted of a series of puncture tests on ABS scales attached onto a soft polyurethane substrate. The geometry and sizes of the scales ($L = 2$ mm, $t = 2$ mm and two different slant angles of $\alpha_0 = 0$ and $\alpha_0 = 63.4^\circ$) as well as the material properties of the substrate ($E_s =$

150 KPa) were identical to those used in the experiments (Martini et al., 2017). In the experiments the elastic modulus of the scales ($E_{ABS} = 3$ GPa (Martini et al., 2017) was four orders of magnitude greater than the substrate. While these values probably differ from the stiffness of the soft tissues surrounding scales in natural dermal armor, they are adequate for the assumption of rigid scales compared to membrane and substrate. We considered the four different configurations shown on Fig. 3a: An isolated scale, and three different 5×5 arrays of scales with small gap distances ($d/L = 0.005$). Each of these models was subjected to a puncture displacement, and the corresponding reaction force was collected to generate a puncture force displacement curve (Fig. 3b). We found good agreement between the model and the experiments in terms of puncture stiffness. The only numerical parameter we calibrated from the puncture experiments was the critical tilt angle which was defined as follows: By puncturing the top surface of the middle scale, the scale started to tilt, and at a critical force the needle starts sliding off the scale into the substrate which is considered as a failure in the system (Shafiei et al., 2021). In the experiments, this event causes a sudden drop in the puncture force on the curve (Fig. 3b). In the numerical model, failure occurs at the end point of the curve where the maximum tilting angle of the top surface of the punctured scale reaches the critical tilting angle. Our previous experiments using an ABS indenter on ABS scales (Martini et al., 2017) indicated a critical angle of $\phi_c = 13^\circ$ for this set of materials, a values which we therefore also used in the model.

3. Puncture resistance of isolated 3D scales

In the following sections of this report we used these validated models to systematically investigate the effects of the 3D scale geometry and arrangement on the response of the system. For this study we focused on scaled skins made of identical scales that were designed to cover a soft substrate entirely. Therefore we only considered scale geometries that tessellate the plane, focusing on the regular triangle, square, isosceles trapezoid, symmetric darts and regular hexagons. To

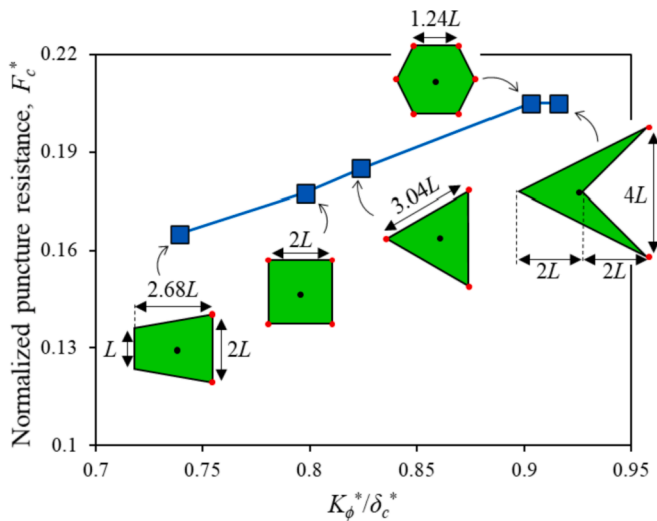


Fig. 4. Puncture resistance of isolated scales with five different base shapes as function of rotational stiffness. All the scales have an equal base area.

isolate the effect of shape, we kept the surface area for the individual scales constant across all models. We first examined the puncture resistance of individual, isolated scales with no slant angle (Fig. 4). Our previous experiments showed that the critical force strongly depends on the location of the puncture on the surface of the scale (Martini et al., 2017). For this study we adopted a conservative approach where for each geometry we puncture the scale at the “worst possible” location, i. e. the location leading to the least puncture resistance. This study therefore provides lower bounds for the puncture resistance of each scaled skin design. For each shape, the “worst case” indentation points produce the longest moment arm δ_c of the puncture force (normalized by $\delta_c^* = \delta_c/L$) from the centroid of the scale, and they are generally located at the corners of the upper surface of the scale (indicated by red dots on Fig. 4).

Fig. 4 shows the puncture resistance F_c normalized by $F_c^* = F_c(1-\nu_s^2)/E_sL^2$ for these five geometries. Closer examination revealed that the puncture resistance is governed by two parameters: the moment arm δ_c created by the indentation force, and the rotational stiffness K_ϕ which is a function of the substrate elasticity and the scale geometry and size

(normalized by $K_\phi^* = K_\phi(1-\nu_s^2)/E_sL^3$). The moment caused by the critical force on the punctured scale is equal to $M^* = F_c^* \times \delta_c^*$, which can also be expressed as $M^* = K_\phi^* \times \phi_c$. By combining these two equations, the puncture resistance therefore is obtained as $F_c^* = \phi_c (K_\phi^* / \delta_c^*)$ which shows that the puncture resistance is proportional to the ratio of the rotational stiffness over the moment arm. Fig. 4 indeed shows a near-proportional relationship between K_ϕ^* / δ_c^* and puncture resistance. The dart and hexagon shapes show the highest puncture resistance.

4. Puncture resistance of arrays of scales

In the next steps, we considered the puncture resistance of arrays of scales. Fig. 5 shows the different combinations of base shapes and arrangements which we examined. For the shapes of triangle, square and trapezoid, we considered two possible arrangements: “arrayed scales” and “staggered scales”. Other shapes like the dart and the hexagon only had one possible tiling configuration. The corresponding 3D arrays of scales for these designs were created by extruding the 2D patterns along the out-of-plane direction by a distance equal to the thickness of the scales, while creating very small gaps ($d/L = 0.005$) between the 3D scales to avoid convergence issues.

Fig. 6a compares the puncture resistance of systems with different base shapes and different arrangements of scales. To emphasize the effect of scale-scale interactions, we normalized the puncture resistance of each array of scales by the puncture resistance of one isolated scale with the same geometry. As expected, the array of scales produced a significantly increased puncture resistance compared to isolated scales, with improvements by factors of 4 to 8. The highest improvements were for the hexagonal and dart scales, which were 20–30% higher than the rest of the designs. Closer examination of the models made it evident that surrounding the indented scales with other scales stabilizes the indented scale. More specifically, the interactions of the scales by direct contact and through the substrates increase the rotational stiffness of the indented scales, with the effect of delaying tilting and increasing puncture resistance. To highlight these effects, we ran additional models where we turned off the contact algorithm, that is scale-to-scale interpenetrated without producing any contact force. The scales could still however interact elastically through the substrate. Even when direct contact was turned off, scales directly neighboring the indented scales (marked by orange dots on Fig. 6a) still had a significant stabilizing effect on the indented scale, while scales further away had negligible effects. These effects were assessed by examination of the coupling

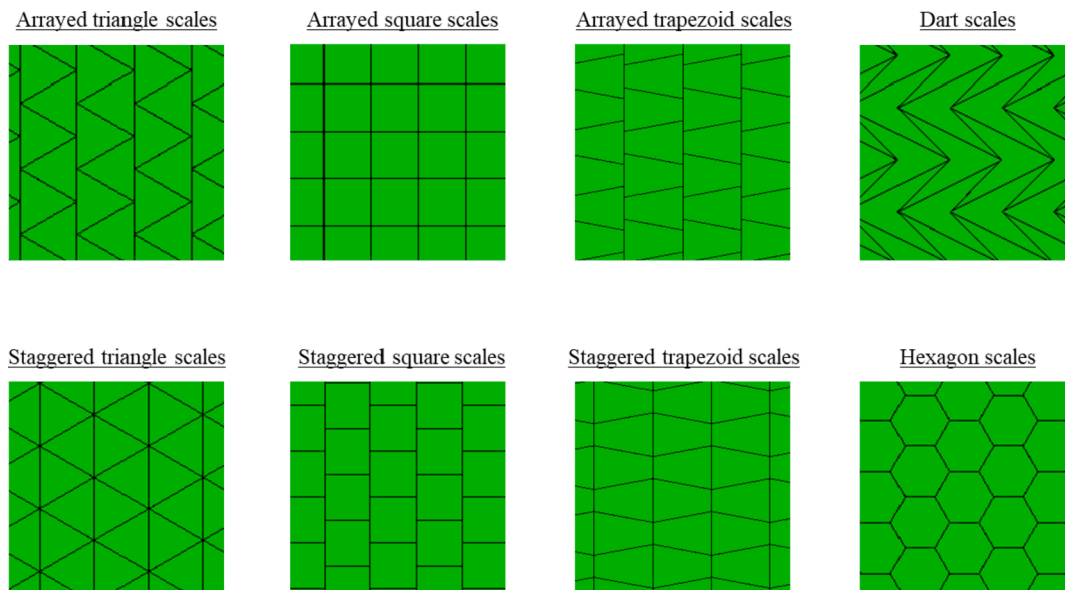


Fig. 5. Eight designs for the base shape and arrangements we considered in this study.

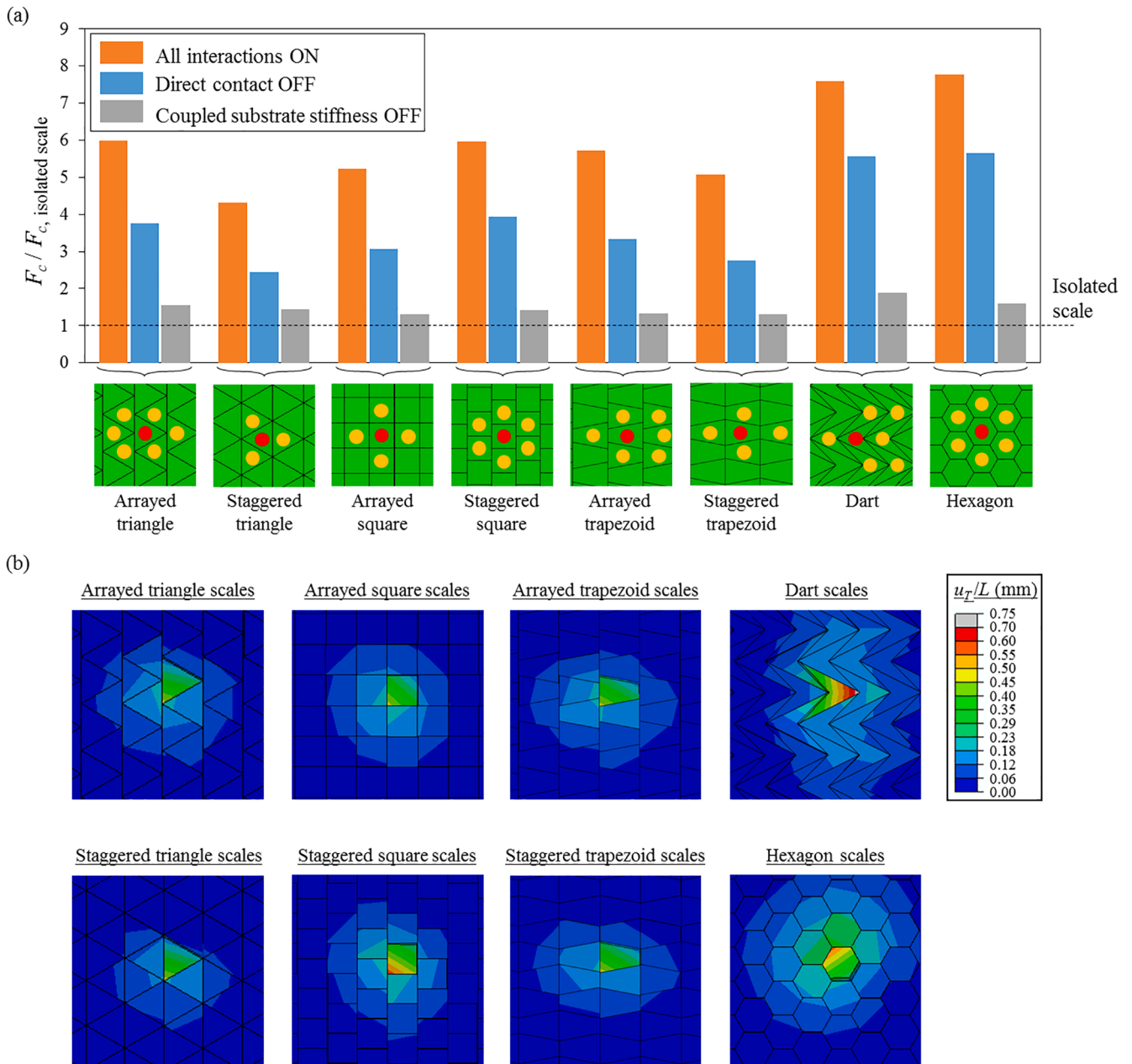


Fig. 6. (a) Puncture resistance for eight different scale arrays normalized by the puncture resistance of an isolated scale with the same geometry. For each design, results with full interaction and only partial interaction through substrate or through direct contact are shown. The punctured scales are marked with red dots, and the effective neighboring scales are marked by orange dots; (b) the displacement distribution in the complete model at the point where the punctured scale reached the critical tilting angle. (For interpretation of the references to colour in this figure legend, the reader is referred to the web version of this article.)

stiffness for each neighboring scales, where a coupling stiffness larger than $K_{li} / K_{0i} > 0.01$ was considered effective. The designs that promoted effective neighbour interactions in terms of number of interactions and configuration produced higher puncture resistances (blue columns on Fig. 6a). Dart- and hexagon-shape scales were the most effective in this regard, increasing the puncture resistance by almost six times of magnitude compared to the isolated-scale models. To further establish the various contributions to puncture resistance, we ran a third set of models where this time direct scale-to-scale contact was enabled, but where the scale to scale interaction stiffness *through* the substrate mostly turned off (the corresponding stiffness terms were reduced to 4% of their original value, further reductions creating convergence issues). In this set of models the scales therefore mainly interacted by direct contact. Fig. 6a (grey columns) shows that all puncture resistances in this set of models are significantly lower than the other sets, with

puncture resistance barely above the puncture resistance of isolated scales. This indicates an important and unexpected feature of the puncture mechanism: neighboring scales stabilize the indented scale predominantly by elastic interaction through the substrate, but by a much lesser extent by direct interaction between the scales (at least with non-slanted sides). Finally, we note that scale-scale interactions not only delay the tilting of the indented scale, but also distributes the load over a larger area (Fig. 6b). Because mechanical interactions were more pronounced for dart- and hexagon-shape scales, the re-distribution of the puncture load over wide area was more effective for these geometries. Fig. 7. Fig. 8. Fig. 9.

By examining the displacements of the scales near the puncture site we identified another mechanism where the scales generate interlocking, preventing the collective motion of groups of scales in the in-plane direction. The interlocking mechanism functions differently in

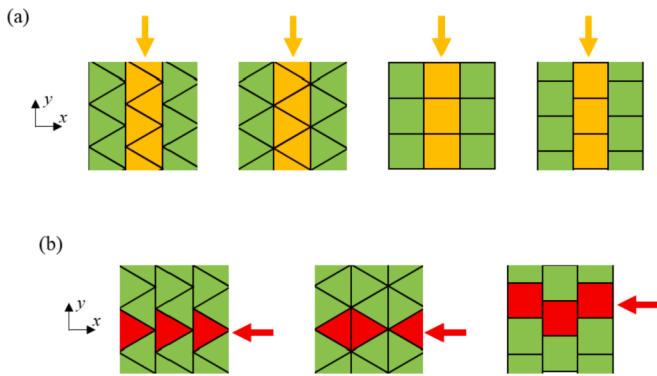


Fig. 7. In-plane sliding of rows of scales may be (a) kinematically allowed by the shape and arrangement of the scales or (b) prevented because of interlocking.

different in-plane directions. Fig. 7a shows examples where in some models a row of scales in y -direction can easily slide against the neighbouring rows with no constraint from contact. On the other hand, shown in Fig. 7b, a row of scales in x -direction hinders the movement of the neighboring rows in this direction by contact (scales are interlocked). These mechanisms are illustrated for triangular and square scales, but they were also observed for trapezoid scales, hexagonal scales and dart scales. This interlocking mechanism engages a larger number of scales, which therefore can improve the puncture resistance of the system. In the “arrayed square scales” model, the free motion of the rows of scales is seen in both x - and y -directions, while the interlocking mechanism occurs along the diagonal ($x = y$) of the scale. In the “dart scales” and “hexagon scales” models, the interlocking mechanism exists in any in-plane directions, which is considered as an advantage in terms of resistance against tilting (will be discussed next).

5. Effects of slant angles in arrays of scales

The previous section discusses how the effects of direct contact for the case of non-slanted scales with straight sides is small, but this effect can be increased by slanting the sides of the scales. In this section we explored the mechanics of arrays of scales with a slant towards three possible directions (Fig. 8): a slant angle of $\alpha_0 = 60^\circ$ towards the x -direction, a slant angle of $\alpha_{45} = 60^\circ$ towards the diagonal ($x = y$) direction, and a slant angle of $\alpha_{90} = 60^\circ$ towards the y -direction.

Fig. 9a displays results from models with full interaction and shows that slanting the scales towards any of the three directions (α_0 , α_{45} and α_{90}) roughly doubles the puncture resistance. This added stabilization effect can be explained by the slant angle changing the direction of the contact force towards the vertical direction, so this force generates a higher moment about the center of the scale. Slanted designs also result

in more scales involved in the puncture mechanism through direct contact mechanism. The results show that slant angle in specific directions are more effective than others. Giving a slant angle to the scales toward the x -direction promotes interlocking, which results in a high puncture resistance. The “arrayed square scales” model with $\alpha_{45} = 60^\circ$ shows the highest resistance against tilting compared to the other slant angles (α_0 and α_{90}), since the interlocking mechanism occurs along the diagonal ($x = y$) of the scale. Finally, Fig. 9a and 9b show that the dart shape and hexagon shapes have a superior puncture resistance because the interlocking mechanism occurs over multiple directions and between a large number of scales.

6. Flexural response

In addition to puncture resistance, flexural compliance is another important criterion for flexible protective system. In this section, we created numerical models to investigate the effect of the base shape, the arrangement and the slant angle of the scales on the overall flexural compliance of the scaled skin. We used the same modeling configuration as in section 2 to create the scales, but this time the scales were bonded onto a membrane composed of linear elastic 8-nodes brick elements (since the membrane is too thick to be considered as a shell, it is not valid to replace it with simple springs.). The elements (type C3D8R) were assigned a modulus E_m and a Poisson’s ratio ν_m , and the model was assigned a very small gap distance of $d/L = 0.005$ (Fig. 10a and b). We built a $10L \times 10L \times 1.5L$ membrane placed in a three-point bending with a support span length of $8L$. Our first task were to duplicate our flexural experiments (Martini et al., 2017) and for this purpose we used $E_m = 700$ kPa, $\nu_m = 0.5$, $L = 2$ mm and $t = 2$ mm. The scaled membrane was loaded in flexion by a narrow rigid plate (Fig. 10a and b) aligned either with the x -direction (Fig. 10a) or with the y -direction (Fig. 10b).

The model predictions in terms of force–deflection are compared with the experiments (from (Martini et al., 2017) in Fig. 11. No fitting procedure or calibration of parameters was used for this comparison, and the predicted force–deflection curves show a good agreement with the experimental results (Fig. 11b and d).

The flexural model can now be extended to other base shapes. Fig. 12 shows the normalized flexural compliance C_f^* (normalized by $C_f^* = C_f E_m I_m / L^3$ where I_m is the second moment of the area of the membrane) for the models with different combinations of base shapes, slant angles and arrangements.

Compared to an isolated scale because of the very small gap distance between the scales and also the direct contact, the scales limit the flexion of the membrane, and as a result the flexural compliance in all the scaled systems decreases by 85% – 93%. The dart is the shape with the largest geometrical size, and therefore for this shape the stiffening in flexion was more pronounced than for the other shapes. Moreover, the interlocking mechanism which is more pronounced in the “dart scales” was beneficial to puncture performance, but our results show that it is

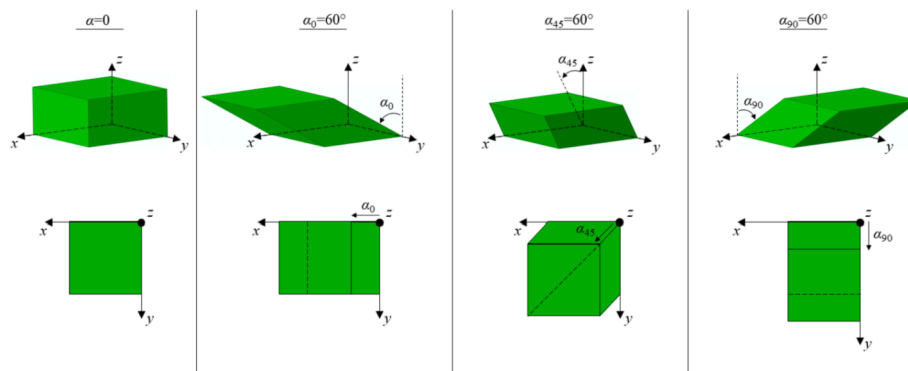


Fig. 8. Starting from scales with straight faces, we considered 60° slant angles towards three different directions.

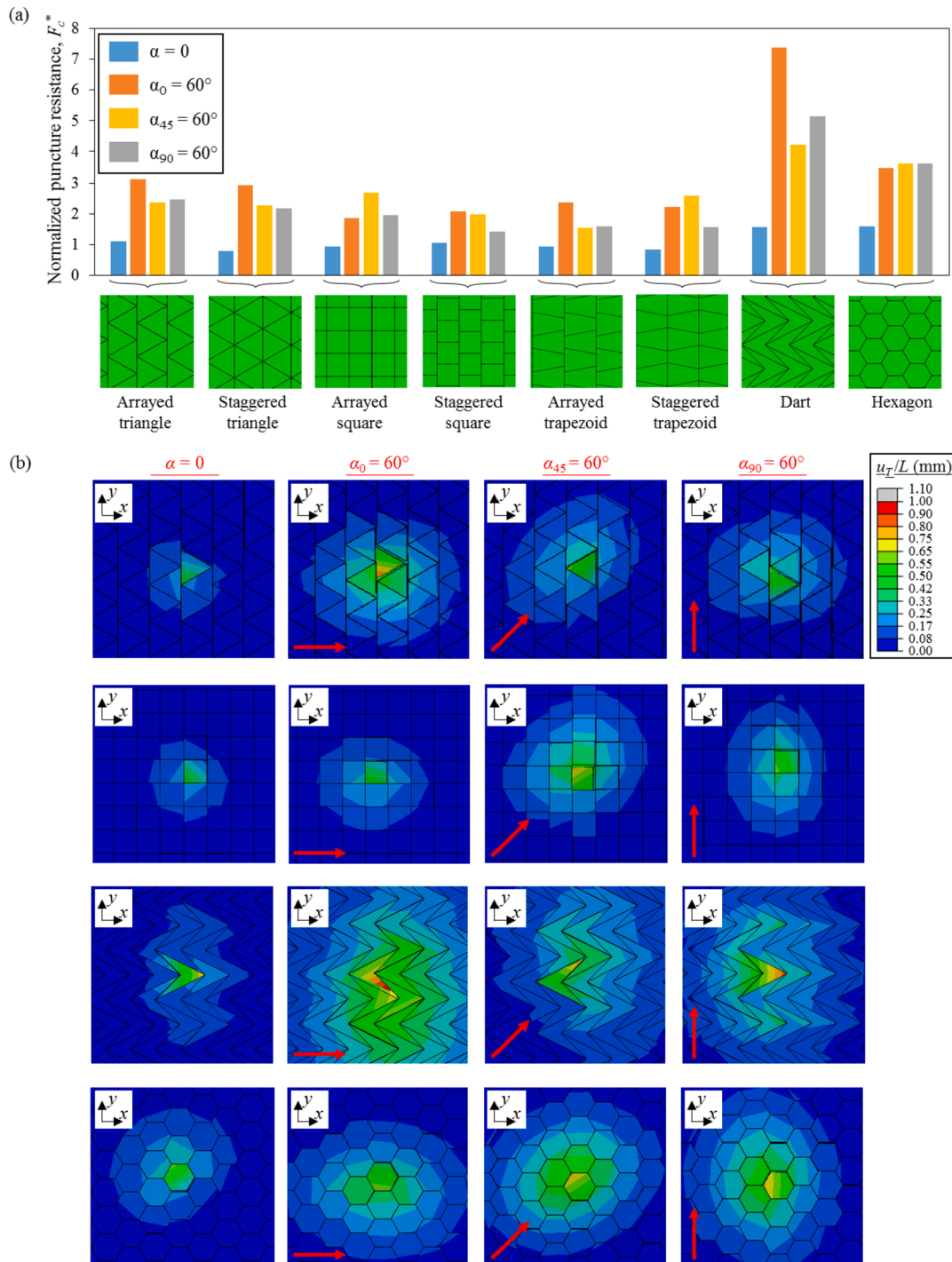


Fig. 9. (a) Puncture resistance of arrays of scales (Note that the normalization used here is different from the one used in Fig. 6). Within each design the effect of slant angle is also shown; (b) In-plane displacement maps for these designs. The red arrows show the direction of the slant angle. (For interpretation of the references to colour in this figure legend, the reader is referred to the web version of this article.)

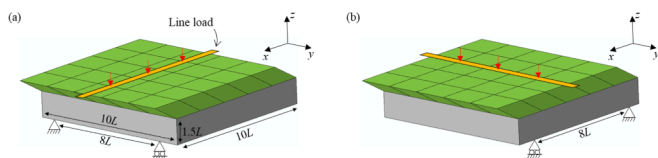


Fig. 10. Configuration for the three-point bending (experiments and models). We considered two orientations for the loading pin (load line): (a) parallel to x -direction and (b) parallel to y -direction.

detrimental to flexural compliance. This observation, along with similar trends from other scale geometries, confirms that puncture resistance and flexural compliance are mutually exclusive (Yang et al., 2013; Martini and Barthelat, 2016; Browning et al., 2013; Martini et al., 2017; Rudykh et al., 2015; Shafiei et al., 2021). The results (Fig. 12) also show that for design purpose, the orientation that we set the three-point bending configuration must be considered, because depending on the orientation, the models show different flexural response. If the direction of the slant angle is parallel to the orientation of the line load the system shows a higher flexural compliance, while the lowest flexural

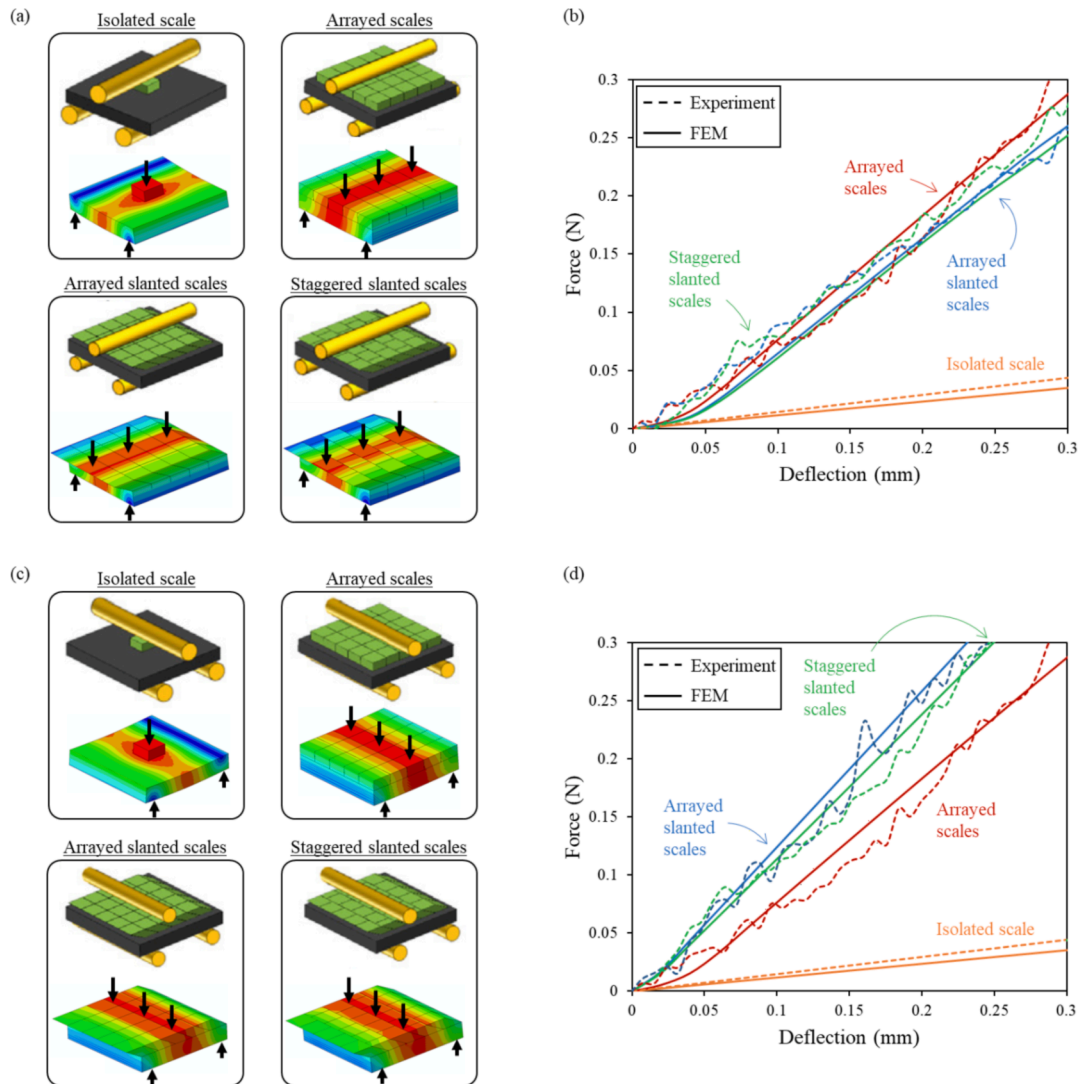


Fig. 11. (a) Three-point flexural tests (diagrams and DEM results) on arrays of scales bonded onto a soft membrane where the line load is parallel to x-direction and (b) corresponding force deflection curves from experiments and DEM models, showing good agreements; (c) Same test with the line load parallel to y-direction with (d) corresponding force deflection curves from experiments and DEM models also showing good agreements.

compliance happens when the slant angle direction is perpendicular to the line load orientation.

7. Summary

In this study we explored the mechanisms of puncture and flexural deformation in soft substrates and membranes covered with rigid scales of various shapes and arrangements. The discrete element modeling approach we used for this work was validated with puncture and flexural experiments. This modeling method brought more insights than the experiments, because a broader range of geometries and interaction parameters could be used, and the mechanisms involved in puncture and flexion could be explored with greater details. Our main findings are as follow:

- For scales with no slant angles, the puncture resistance increases mainly by elastic interactions through the substrate, and with much less extent by direct contact between the scales.
- The interlocking mechanism between rows of scales plays an important role in engaging a larger number of scales during loading, which results in a higher puncture resistance

- Slant angle towards any directions improve the puncture resistance of the system, however, a slant angle towards the direction with interlocking mechanism makes the effect of the slant angle more pronounced.
- Dart- and hexagon-shape scales show the best performance in terms of puncture resistance compared to the other models
- To have a better flexural performance, the direction of the slant angle must be considered parallel to the orientation of the three-point bending configuration

This exploration of mechanisms finally produced a comparative database of the flexure-compliance performance of various designs, which can be conveniently summarized using the Ashby chart showed on Fig. 13.

Isolated scale (with any base shapes) shows the highest flexural compliance but the puncture resistance is the lowest. Covering the substrate with scales improves the puncture resistance, but, at the cost of low flexibility. Simple system of “arrayed square scales” with no slant angles ($\alpha = 0$) increases the puncture resistance by five times. By only giving a slant angle of $\alpha_{45} = 60^\circ$ to the scales, we can improve the puncture resistance even more by about three times of the model with no slant angle. Changing the base shape of the scales also has a significant

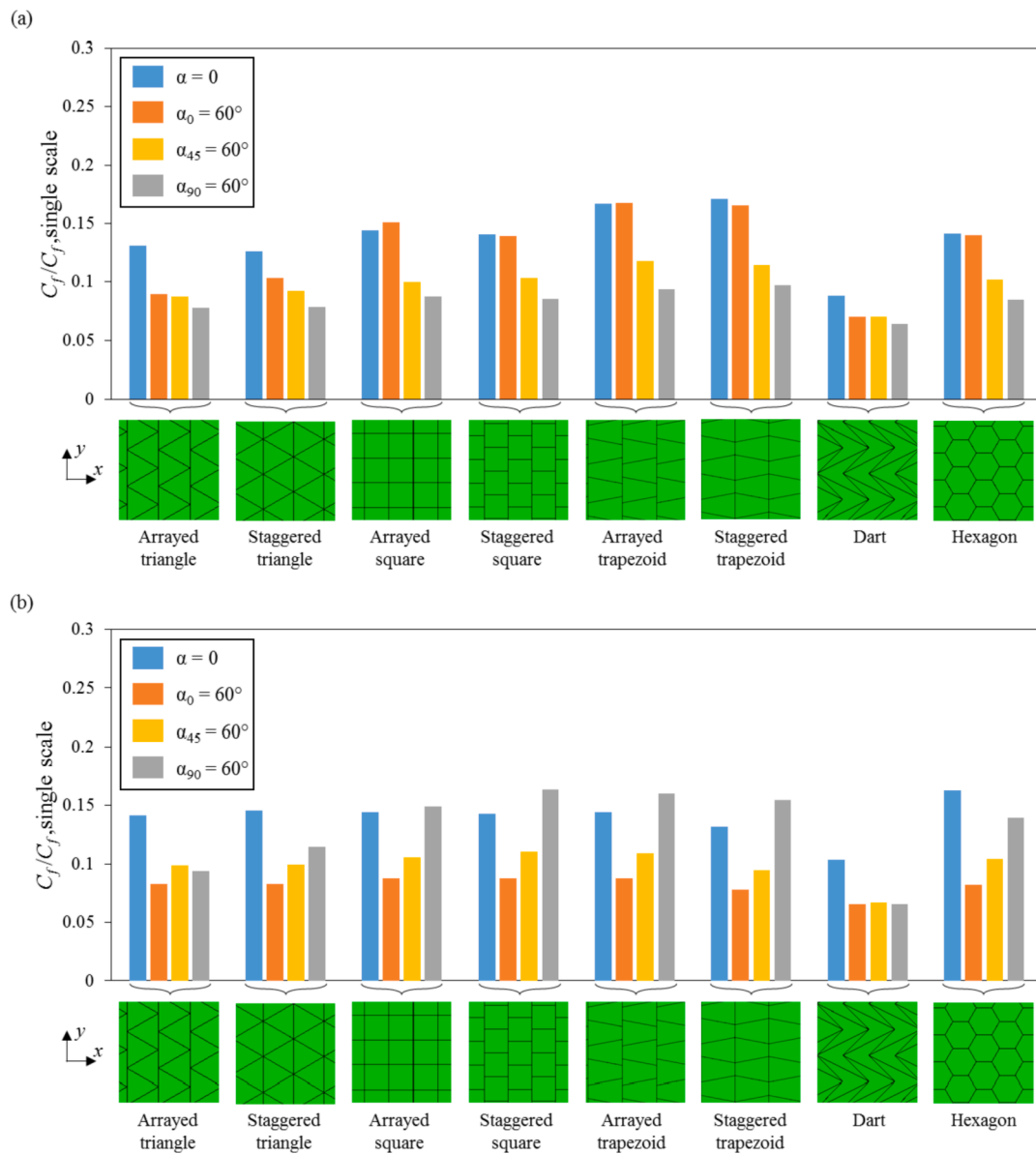


Fig. 12. Flexural compliance of arrays of scales on soft membrane with different combinations of base shapes, slant angles and arrangements and where the line load is applied (a) parallel to the x-direction and (b) parallel to the y-direction.

effect on puncture resistance. When all these effects and mechanisms are combined, the puncture resistance of “dart scales” model with $\alpha_0 = 60^\circ$ slant was about 42 times higher than an isolated scale with the same geometry. This puncture resistance only comes at the cost of a small decrease in compliance compared to the other designs. The “banana shape” of Fig. 13 illustrates the mutually exclusive character of puncture resistance and flexural stiffness, a trend also observed in other studies (Yang et al., 2013; Browning et al., 2013; Rudykh et al., 2015; Shafiei et al., 2021). Although we cannot generalize this result, it is likely that the mutual exclusiveness of puncture resistance and flexural compliance is a universal feature of flexible armor, including in natural scales. For example ancient, near extinct fish with ganoid scale were probably replaced by modern fish with thinner and more flexible scales, to gain maneuverability and higher evasive capabilities at the expense of protection.

This study provides new insights into the effect of the base shape and the slant angle of the scales on the mechanical behavior of a scale-covered system and the interlocking mechanism of the scales, which in turn can help in the design and optimization of improved protective

systems. In this study we considered a range of convex and angular geometries for the scales which we kept relatively simple to control the scope of the exploration and gain basic insights into scale interactions in 3D. Using the same modeling approach, these geometries could be further enriched with rounded edges or concave features that could further promote interlocking. Complex geometries such similar to natural ganoid scales are beyond the scope of this study, but could also be captured using this modeling approach to capture interlocking and collective deformation mechanism in this natural armor. Another parameter of potential interest is friction between the scales. In the models presented here we used frictionless contact in order to focus on geometrical effects that could resist the relative motion of the scales. Adding friction to the contact interaction would impede scale-scale sliding further, but major effects and trends related to geometry would probably be unchanged. In practice friction could be increased by manipulating the surface of the scales, which could be considered in future models. Future work could include nonlinear substrate and friction between the scales, which would allow to capture more extreme deformations, possibly revealing additional mechanisms of interaction

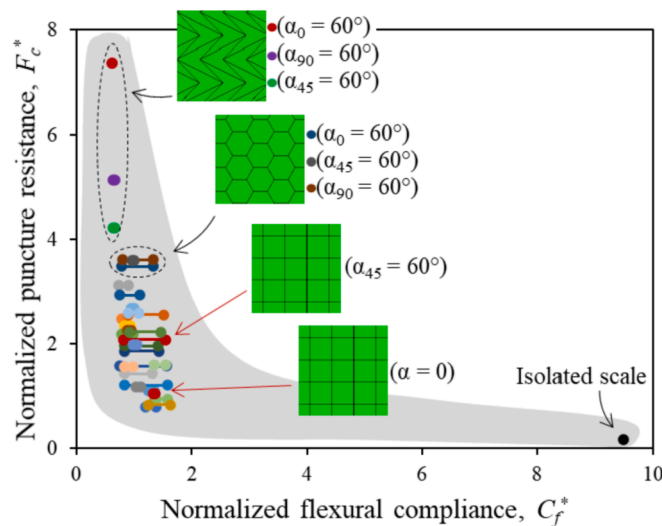


Fig. 13. Ashby chart showing the normalized puncture resistance and the normalized flexural compliance for different combinations of base shapes, slant angles and arrangements.

between scales and substrate, and potentially leading to additional insights into this system.

Declaration of Competing Interest

The authors declare that they have no known competing financial interests or personal relationships that could have appeared to influence the work reported in this paper.

Acknowledgements

This work was supported by a Discovery Grant from the Natural Sciences and Engineering Research Council of Canada. A.S. was partially supported by a McGill Engineering Doctoral Award.

References

- Wegst, U.G.K., et al., 2014. Bioinspired structural materials. *Nat. Mater.* 14, 23.
- Chen, P.-Y., McKittrick, J., Meyers, M.A., 2012. Biological materials: Functional adaptations and bioinspired designs. *Prog. Mater. Sci.* 57 (8), 1492–1704.
- Rajabi, H., Shafiei, A., Darvizeh, A., Dirks, J.-H., Appel, E., Gorb, S.N., 2016. Effect of microstructure on the mechanical and damping behaviour of dragonfly wing veins. *R. Soc. Open Sci.* 3 (2), 160006. <https://doi.org/10.1098/rsos.160006>.
- Chen, I.H., Kiang, J.H., Correa, V., Lopez, M.I., Chen, P.-Y., McKittrick, J., Meyers, M.A., 2011. Armadillo armor: Mechanical testing and micro-structural evaluation. *J. Mech. Behav. Biomed. Mater.* 4 (5), 713–722.
- Barthelat, F., 2015. Architected materials in engineering and biology: fabrication, structure, mechanics and performance. *Int. Mater. Rev.* 60 (8), 413–430.
- Chintapalli, R.K., Mirkhalaf, M., Dastjerdi, A.K., Barthelat, F., 2014. Fabrication, testing and modeling of a new flexible armor inspired from natural fish scales and osteoderms. *Bioinspiration Biomimetics* 9 (3), 036005. <https://doi.org/10.1088/1748-3182/9/3/036005>.
- Zhu, D., Ortega, C.F., Motamedi, R., Szweciw, L., Vernerey, F., Barthelat, F., 2012. Structure and Mechanical Performance of a “Modern” Fish Scale. *Adv. Eng. Mater.* 14 (4), B185–B194.

- Yang, W., Chen, I.H., Gludovatz, B., Zimmermann, E.A., Ritchie, R.O., Meyers, M.A., 2013. Natural Flexible Dermal Armor. *Adv. Mater.* 25 (1), 31–48.
- Vernerey, F.J., Barthelat, F., 2014. Skin and scales of teleost fish: Simple structure but high performance and multiple functions. *J. Mech. Phys. Solids* 68, 66–76.
- Rudykh, S., Boyce, M.C., 2014. Analysis of elasmoid fish imbricated layered scale-tissue systems and their bio-inspired analogues at finite strains and bending. *IMA J. Appl. Math.* 79 (5), 830–847.
- Szweciw, L., Barthelat, F., 2017. Mechanical properties of striped bass fish skin: Evidence of an extendon function of the stratum compactum. *J. Mech. Behav. Biomed. Mater.* 73, 28–37.
- Vernerey, F.J., Musiket, K., Barthelat, F., 2014. Mechanics of fish skin: A computational approach for bio-inspired flexible composites. *Int. J. Solids Struct.* 51 (1), 274–283.
- Vernerey, F.J., Barthelat, F., 2010. On the mechanics of fishscale structures. *Int. J. Solids Struct.* 47 (17), 2268–2275.
- Ghosh, R., Ebrahimi, H., Vaziri, A., 2014. Contact kinematics of biomimetic scales. *Appl. Phys. Lett.* 105 (23), 233701. <https://doi.org/10.1063/1.4903160>.
- Ghosh, R., Ebrahimi, H., Vaziri, A., 2016. Frictional effects in biomimetic scales engagement. *EPL (Europhysics Letters)* 113 (3), 34003. <https://doi.org/10.1209/0295-5075/113/34003>.
- Martini, R., Barthelat, F., 2016. Stretch-and-release fabrication, testing and optimization of a flexible ceramic armor inspired from fish scales. *Bioinspiration Biomimetics* 11 (6), 066001. <https://doi.org/10.1088/1748-3190/11/6/066001>.
- Zhu, D., Szweciw, L., Vernerey, F., Barthelat, F., 2013. Puncture resistance of the scaled skin from striped bass: Collective mechanisms and inspiration for new flexible armor designs. *J. Mech. Behav. Biomed. Mater.* 24, 30–40.
- Browning, A., Ortiz, C., Boyce, M.C., 2013. Mechanics of composite elasmoid fish scale assemblies and their bioinspired analogues. *J. Mech. Behav. Biomed. Mater.* 19, 75–86.
- Tatari, M., Kamrava, S., Ghosh, R., Nayeb-Hashemi, H., Vaziri, A., 2020. Bending behavior of biomimetic scale covered beam with tunable stiffness scales. *Sci. Rep.* 10 (1) <https://doi.org/10.1038/s41598-020-74147-0>.
- Funk, N., Vera, M., Szweciw, L.J., Barthelat, F., Stoykovich, M.P., Vernerey, F.J., 2015. Bioinspired Fabrication and Characterization of a Synthetic Fish Skin for the Protection of Soft Materials. *ACS Appl. Mater. Interfaces* 7 (10), 5972–5983.
- Martini, R., Balit, Y., Barthelat, F., 2017. A comparative study of bio-inspired protective scales using 3D printing and mechanical testing. *Acta Biomater.* 55, 360–372.
- Rudykh, S., Ortiz, C., Boyce, M.C., 2015. Flexibility and protection by design: imbricated hybrid microstructures of bio-inspired armor. *Soft Matter* 11 (13), 2547–2554.
- Shafiei, A., Pro, J.W., Martini, R., Barthelat, F., 2021. The very hard and the very soft: Modeling bio-inspired scaled skins using the discrete element method. *J. Mech. Phys. Solids* 146, 104176. <https://doi.org/10.1016/j.jmps.2020.104176>.
- Martini, R., Barthelat, F., 2016. Stability of hard plates on soft substrates and application to the design of bioinspired segmented armor. *J. Mech. Phys. Solids* 92, 195–209.
- Connors, M., et al., 2019. Bioinspired design of flexible armor based on chiton scales. *Nat. Commun.* 10 (1), 5413.
- Ghods, S., et al., 2020. On the regeneration of fish scales: structure and mechanical behavior. *J. Experiment. Biol.* 223 (10).
- Murcia, S., McConville, M., Li, G., Ossa, A., Arola, D., 2015. Temperature effects on the fracture resistance of scales from *Cyprinus carpio*. *Acta Biomater.* 14, 154–163.
- Ghods, S., Murcia, S., Ossa, E.A., Arola, D., 2019. Designed for resistance to puncture: The dynamic response of fish scales. *J. Mech. Behav. Biomed. Mater.* 90, 451–459.
- Dugué, M., Fivel, M., Bréchet, Y., Dendievel, R., 2013. Indentation of interlocked assemblies: 3D discrete simulations and experiments. *Comput. Mater. Sci.* 79, 591–598.
- Ghosh, R., Ebrahimi, H., Vaziri, A., 2017. Non-ideal effects in bending response of soft substrates covered with biomimetic scales. *J. Mech. Behav. Biomed. Mater.* 72, 1–5.
- Abid, N., Mirkhalaf, M., Barthelat, F., 2018. Discrete-element modeling of nacre-like materials: Effects of random microstructures on strain localization and mechanical performance. *J. Mech. Phys. Solids* 112, 385–402.
- Abid, N., Pro, J.W., Barthelat, F., 2019. Fracture mechanics of nacre-like materials using discrete-element models: Effects of microstructure, interfaces and randomness. *J. Mech. Phys. Solids* 124, 350–365.
- Pro, J.W., Barthelat, F., 2020. Discrete element models of fracture in tooth enamel: Failure mode competition and statistical effects. *J. Mech. Phys. Solids* 137, 103868.
- Bolander, J.E., Saito, S., 1998. Fracture analyses using spring networks with random geometry. *Eng. Fract. Mech.* 61 (5-6), 569–591.
- Barber, J.R., 2002. *Elasticity*. Springer.
- Okumura, I.A., 1995. On the generalization of Cerruti’s problem in an elastic half-space. *Doboku Gakkai Ronbunshu* 1995 (519), 1–10.